Топологические дефекты в графене

В.А. Осипов
(БЛТФ, ОИЯИ, Дубна)

Carbon lattices

Sp3

Tetrahedral network

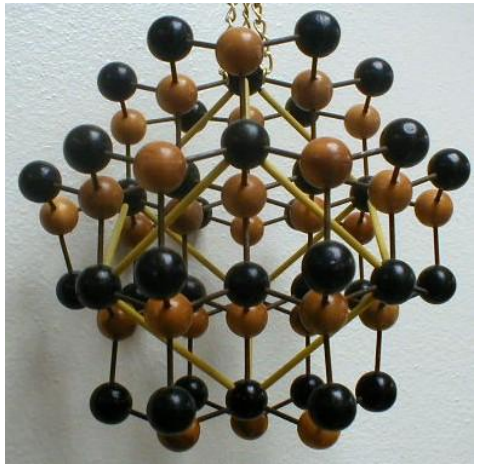

→

strong bonds

Sp2

Hexagonal layers

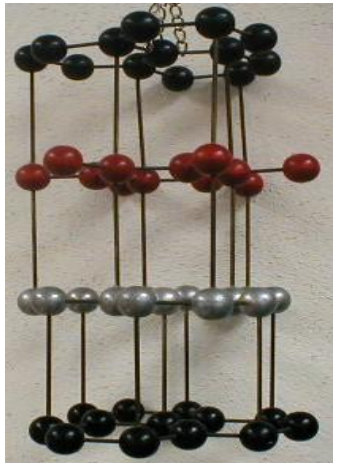

→

weak VDW forces between the layers

Graphene (2005)

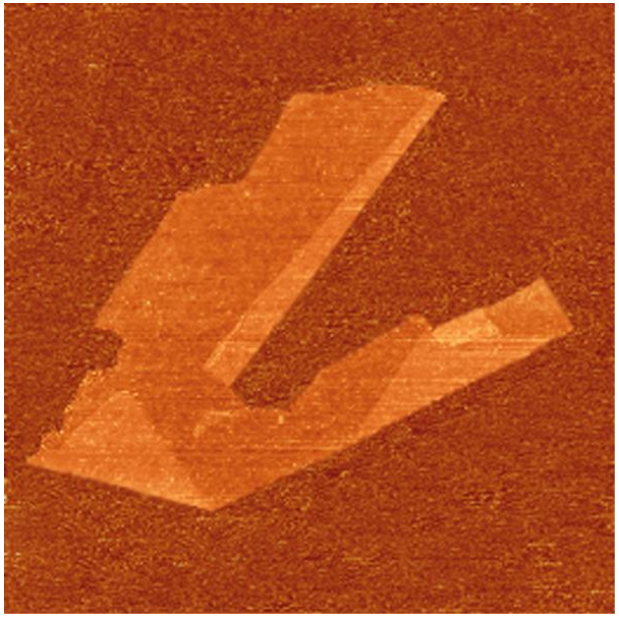

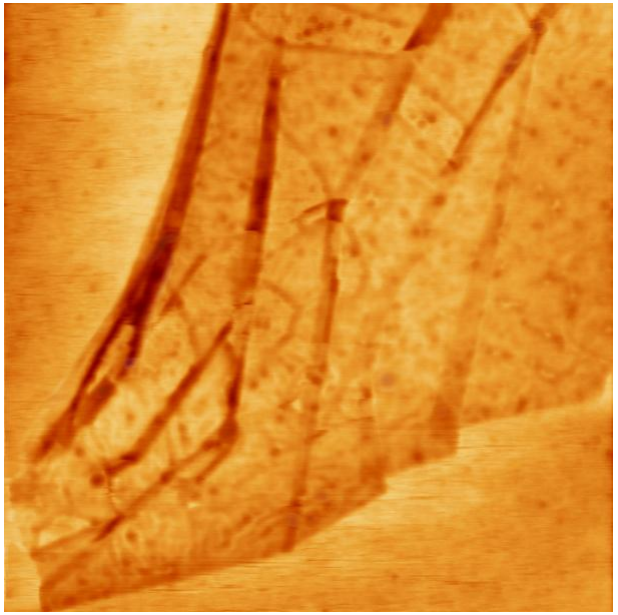

source: site of Mesoscopic Physics Group (Manchester University)

AFM images of: a graphene molecule (left). The window size is 10x10 micron (the graphene film is only one atom thick but approx. 100,000 atoms long in the two lateral directions;

single-atom-thin carbon nanofabric (right) (3x3 micron in size). Graphene looks just like a silk tissue thrown on a surface: it is creased with many folds, pleats and wrinkles.

Nobel Prize in Physics (2010)

A. Geim and

K. Novoselov

for groundbreaking experiments regarding the two-dimensional material graphene

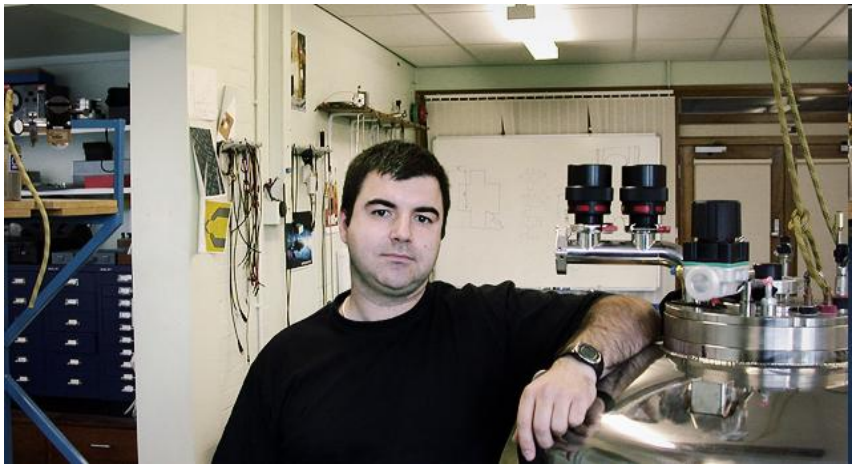


20
The specific of field emission for carb
aboratory of Theoretical Physics, Joi
a, Russia.
sipov JETP Lett., 90, 304 (2009)
ween the number of layers in few-layer
electron energy distribution (FEED).
we known last relation, we can obtain important
um and concrete types of emitting sheets.
quantity of emitted electrons
vs
energy of emitted electrons
when strong
rons from the solid.
h respect to the
rgment
n of FLG
berghaus
Vsevolod Katkov
Dubna, RU

How to create a 2D crystal?

Crystalline Order in Two Dimensions*

N. D. Mermin†
Laboratory of Atomic and Solid State Physics, Cornell University, Ithaca, New York
(Received 1 July 1968)

This result excludes conventional crystalline long-range order in two dimensions

Mermin: "… the bound can be so weak to allow two-dimensional systems of less than **astronomic size** to display crystalline order"

$L<10^{30}m$

Possible explanations on how graphene evades the Mermin-Wagner theorem:

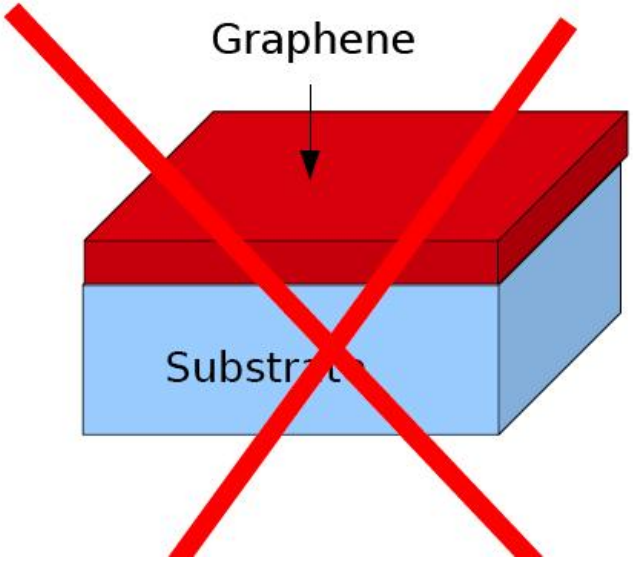

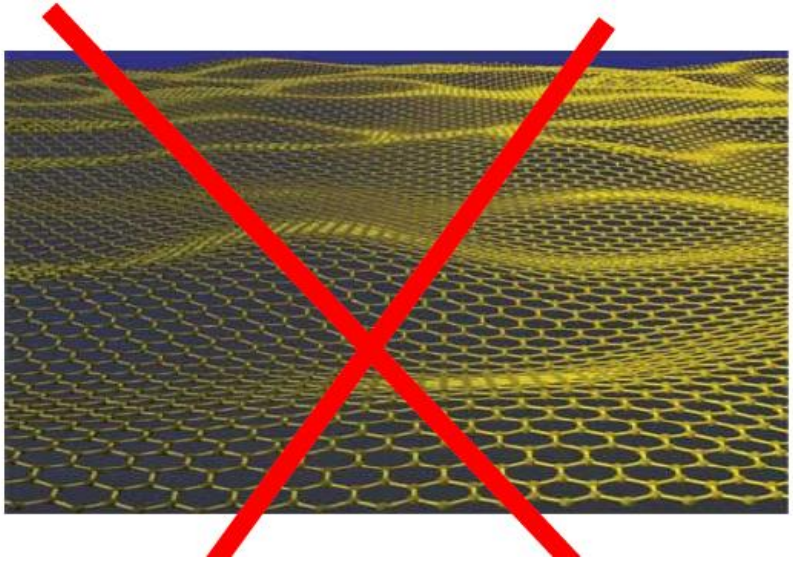

Ribbons

Science **319**, 1229 (2008): Chemical Derivation

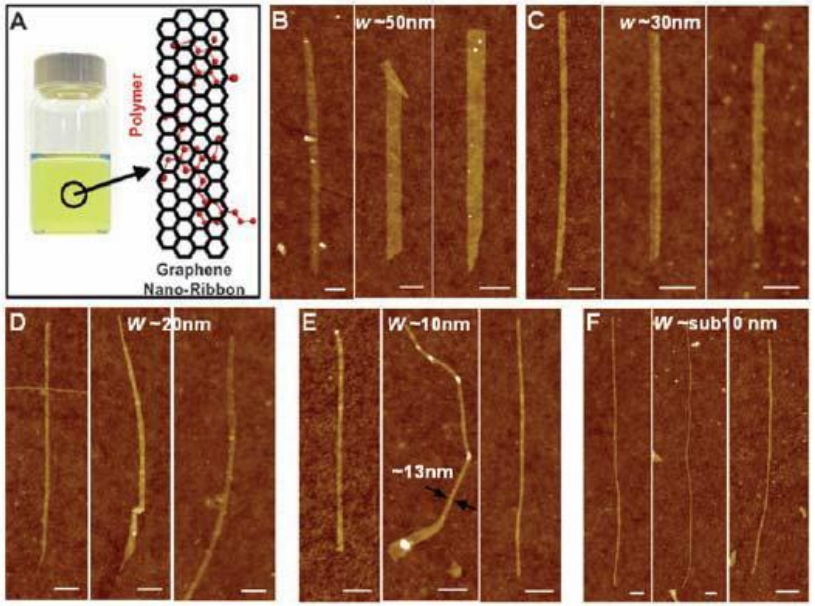

Nature **458**, 872 (2009): SWCNT Unzipping

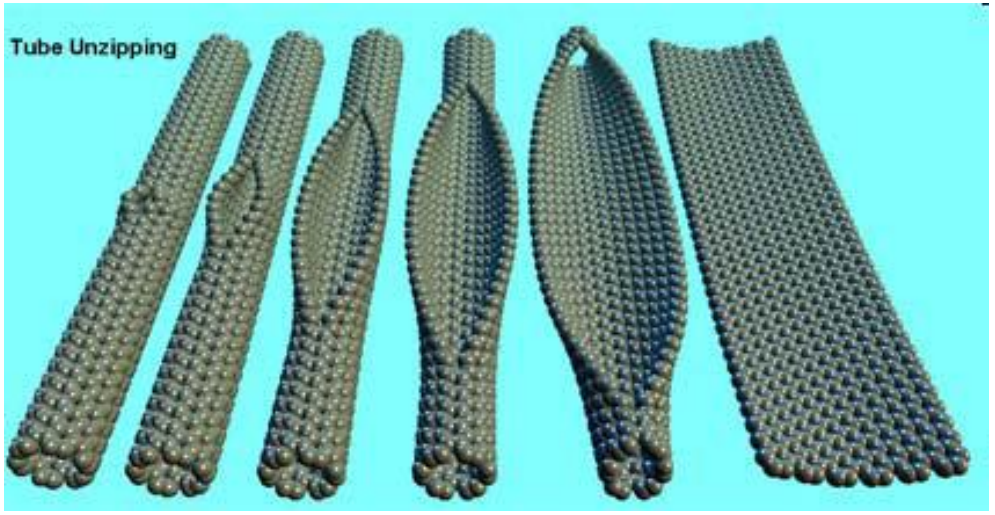

Nature Nanotechnology **3**, 397 (2008): STM Nanolithography

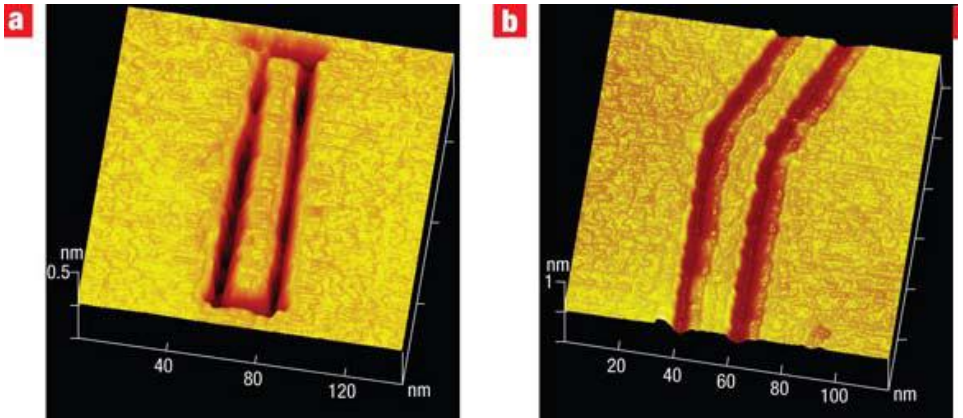

Pentagons and disclination buckling transition

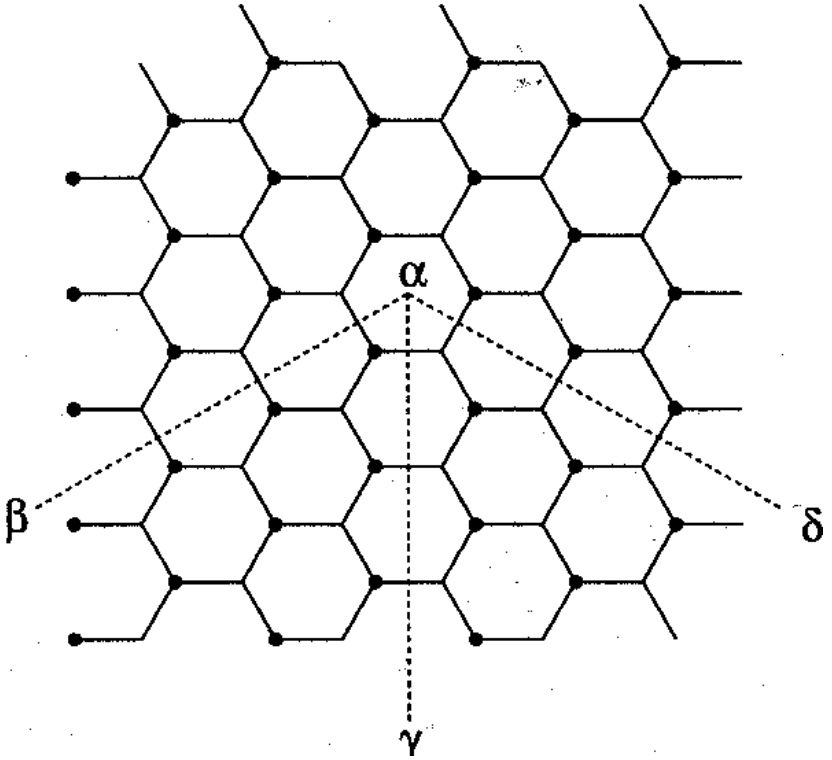

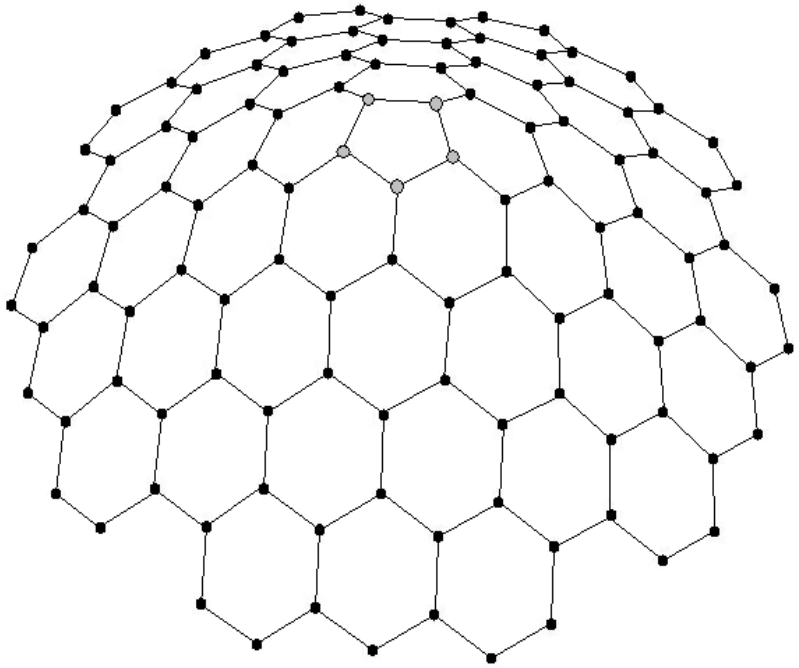

By its nature, the pentagon in a graphite sheet is a topological defect. Actually, fivefold coordinated particles (pentagons) are orientational disclination defects in the otherwise sixfold coordinated triangular lattice.

Defects, Curvature

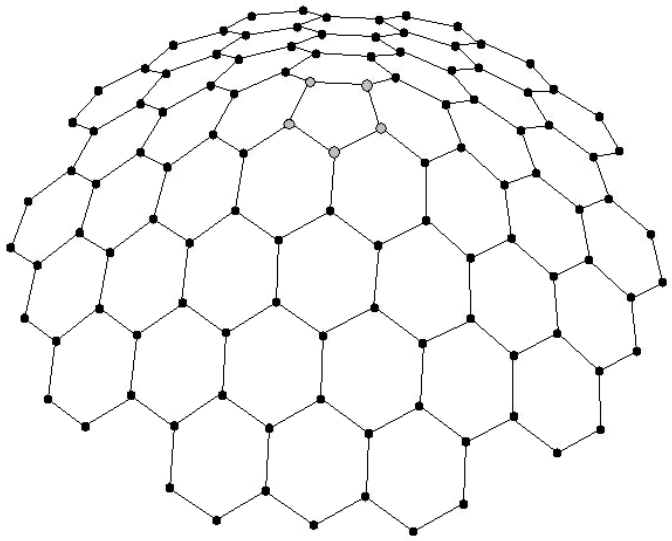

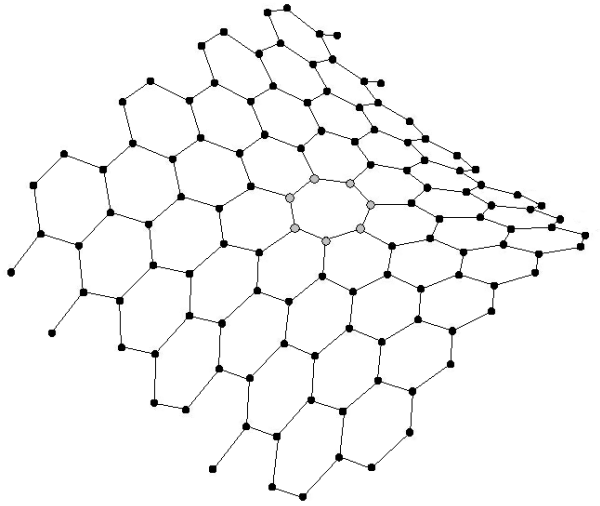

The pentagon (positive curvature) and the heptagon (negative curvature) in the hexagonal graphite lattice

Experimental observation of the pentagon by STM (scanning tunneling microscopy)

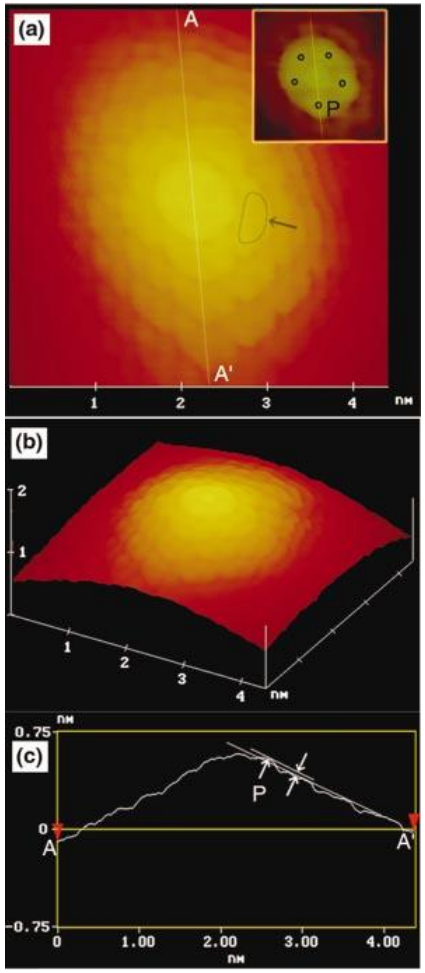

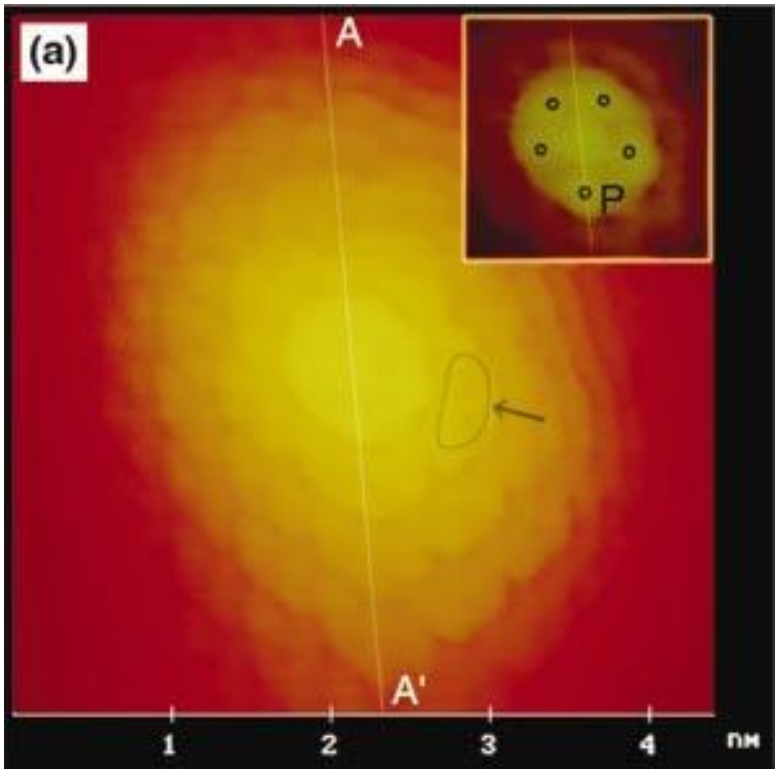

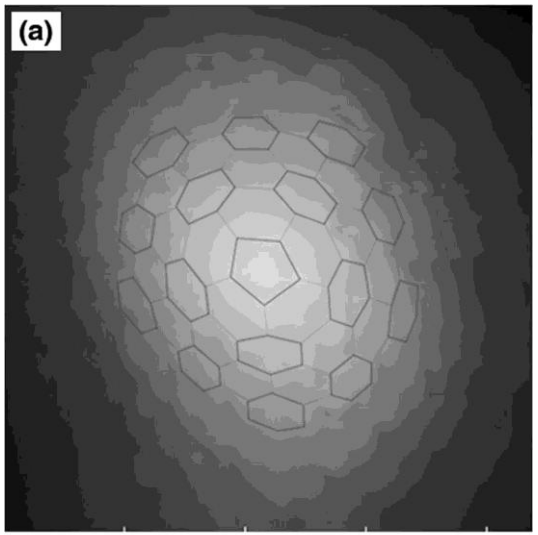

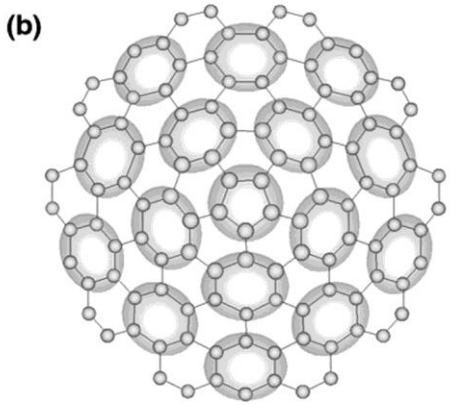

B.An et.al, Appl.Phys.Lett. 78, 3696 (2001): the enhanced charge density localized at each carbon atom in the pentagon was experimentally clarified. Typical images of the conical protuberance by STM: (a) Top view of the apex, (b) Bird's-eye view, (c) Cross section along line AA'. Five bright spots are clearly seen.

Cone geometry

Due to the symmetry of a graphite sheet only five types of cones can be created from a continuous sheet of graphite. The total disclinations of all these cones are multiplies of 60º, corresponding to the presence of a given number (n) of pentagons at the apices.

Important: carbon nanocones with cone angles of 19º, 39º, 60º, 85º, and 113º have been observed in a carbon sample

A. Krishnan et al., Nature (London), **388**, 451 (1997).

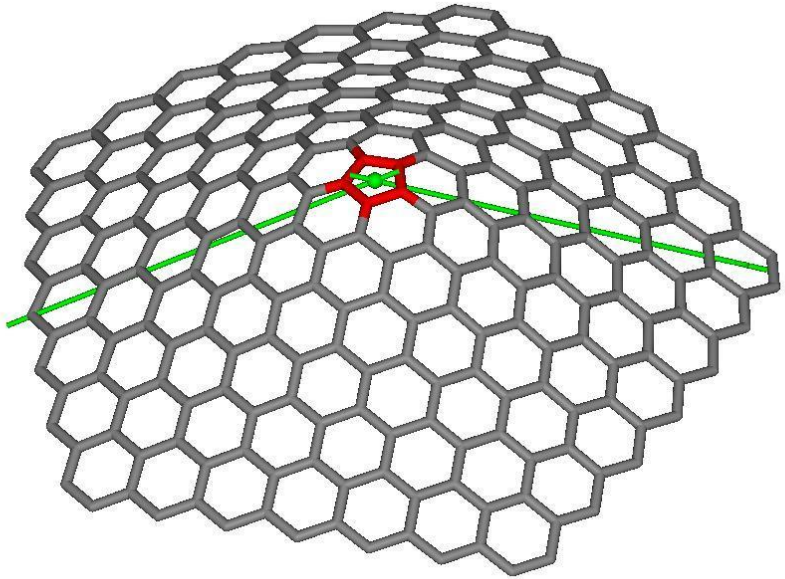

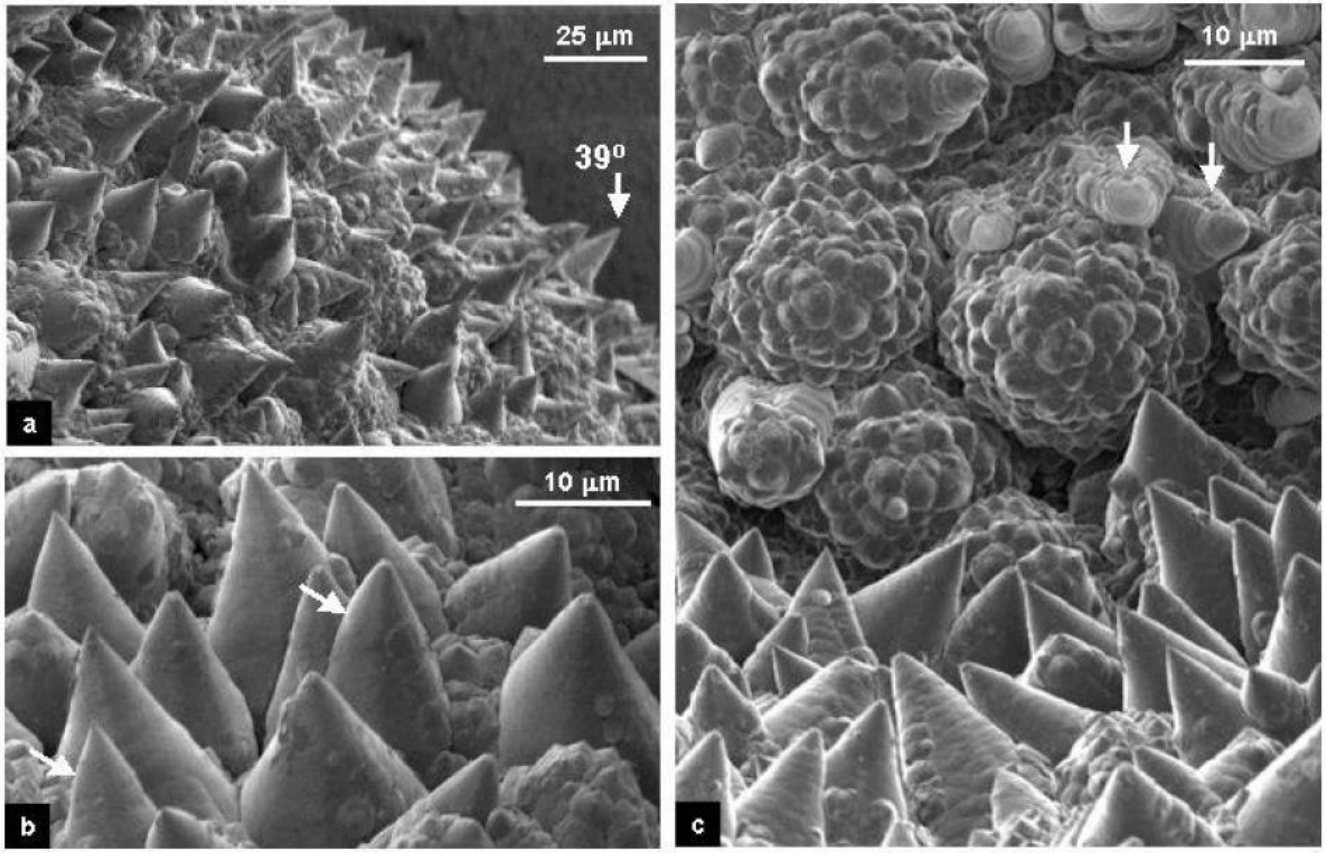

Fig. 2. FESEM images of a cone-covered graphite aggregate. (a) Low-magnification image showing complete coverage of the aggregate surface with conical structures. A ~39° cone is marked by an arrow. (b) Higher magnification image of the sample showing a variety of large cones with different apex angles and sharp and blunt tips. Arrows show changes in the apex angle. (c) Close up view of two surfaces which are almost perpendicular and show different cone morphologies – large cones on one surface and globular (artichoke-like) structures on the other. The latter ones are clusters of large-angle cones. Arrows show some of the cones that are ripped on the side

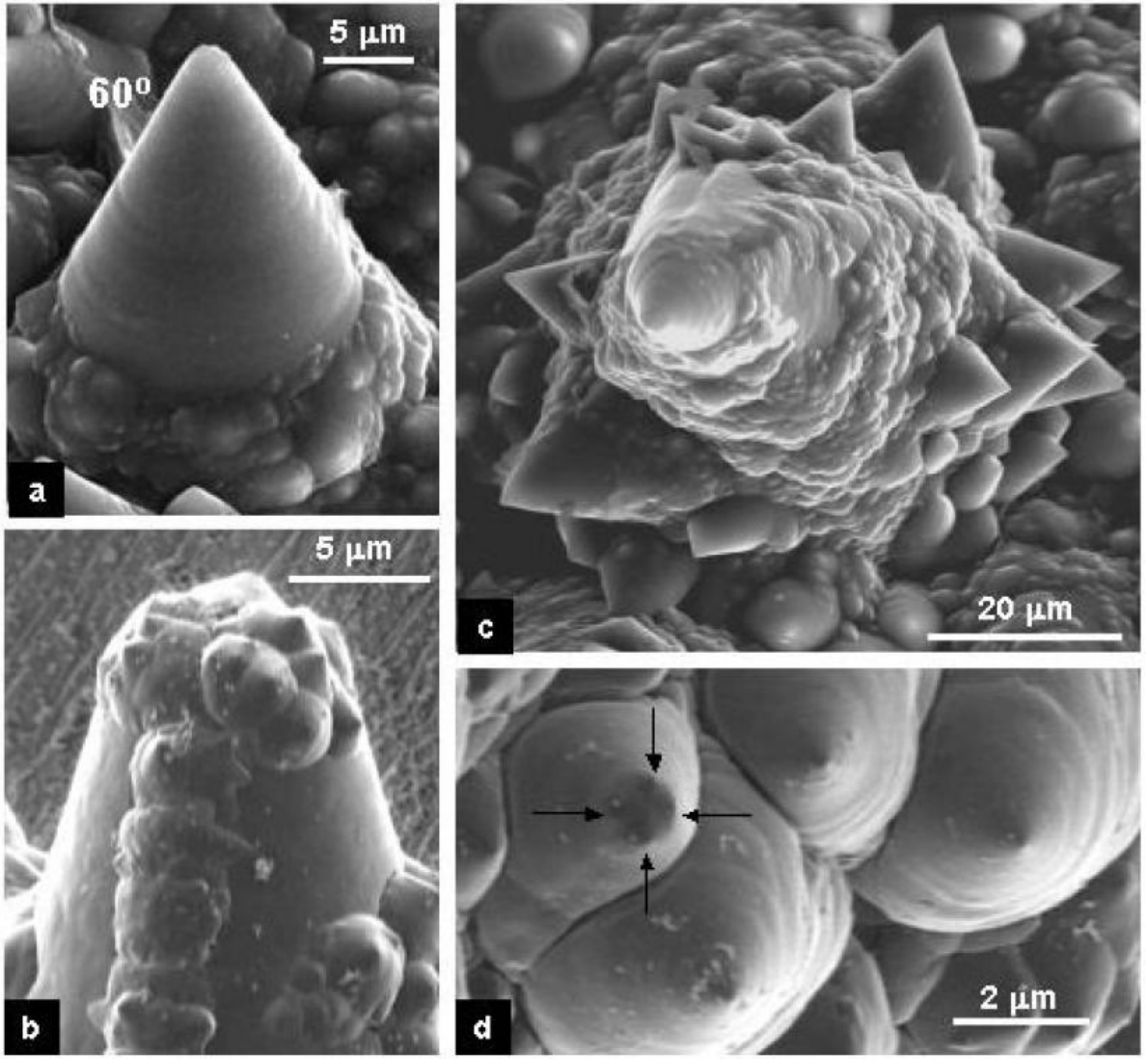

Fig. 3. Typical cone morphologies. (a) SEM image of a cone with a 60° apex angle, the most common apex angle. The slightly uneven surface of the cone suggests layer growth. (b) FESEM and (c) SEM images of large cones with numerous smaller cones growing on their surface. Smaller cones covering surfaces of large cones have a broad distribution of shapes, but large apex angles prevail (c). (d) FESEM image of four cones having sharp and broad tips (multiple tips are marked by arrows). The cones are oriented to reveal their circular cross sections around the tips and layered growth (ripples).

A presence of sharp resonant states in the region close to the Fermi energy

J.-C. Charlier and G.-M. Rignanese, Phys. Rev.Lett. 86, 5970 (2001)

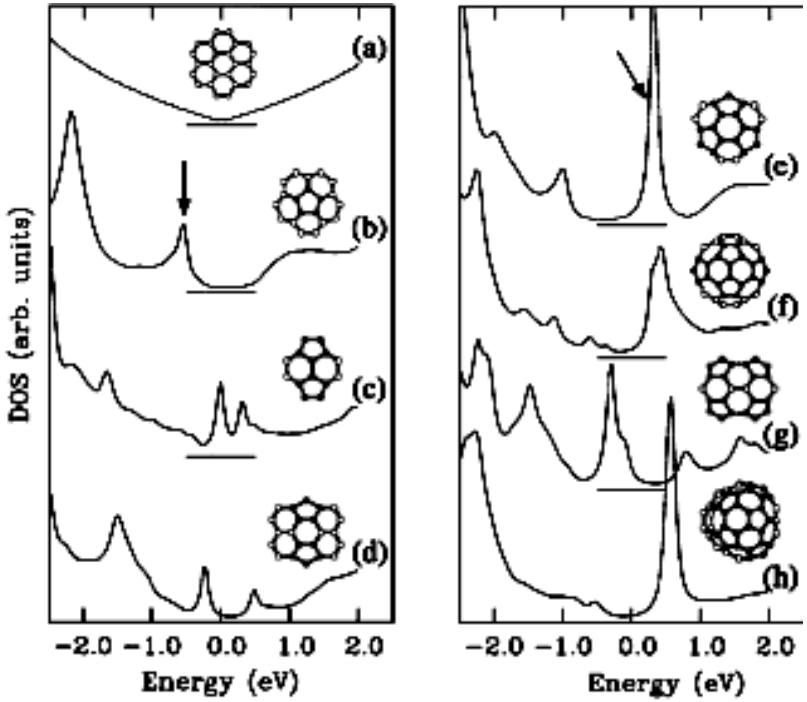

Computed tight-binding LDOS for a single graphene layer (a), and nanocones with one (b), two (c) and (d), three (e), four (f) and (g), and five (h) pentagons, respectively. The Fermi level is at zero energy.

The strength and the position of these states with respect to the Fermi level was found to depend sensitively on the number and the relative positions of the pentagons constituting the conical tip. In particular, a prominent peak which appears just above the Fermi level was found for the nanocone with three symmetrical pentagons (which corresponds to a 60˚ opening angle or, equivalently, to 180˚ disclination).

Nanohorns

Source: S. Berber et al., Phys.Rev.B 62, R2291 (2000)

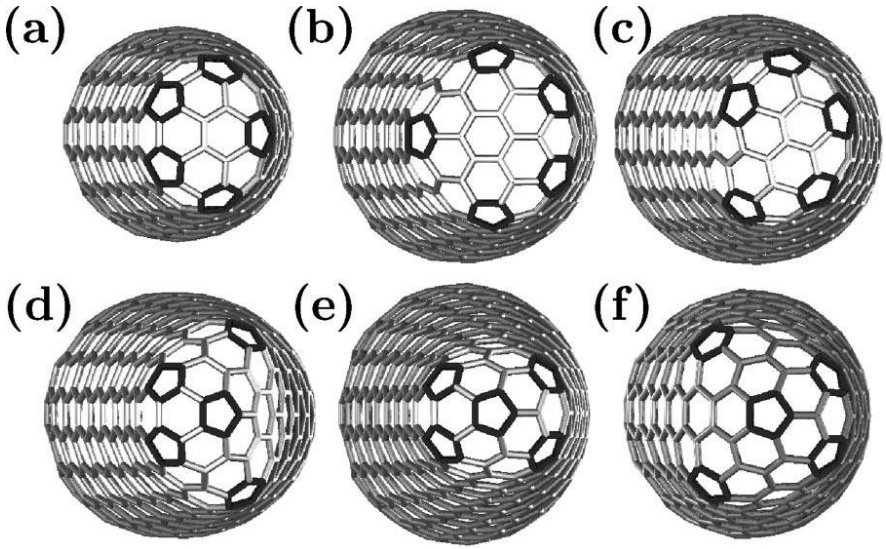

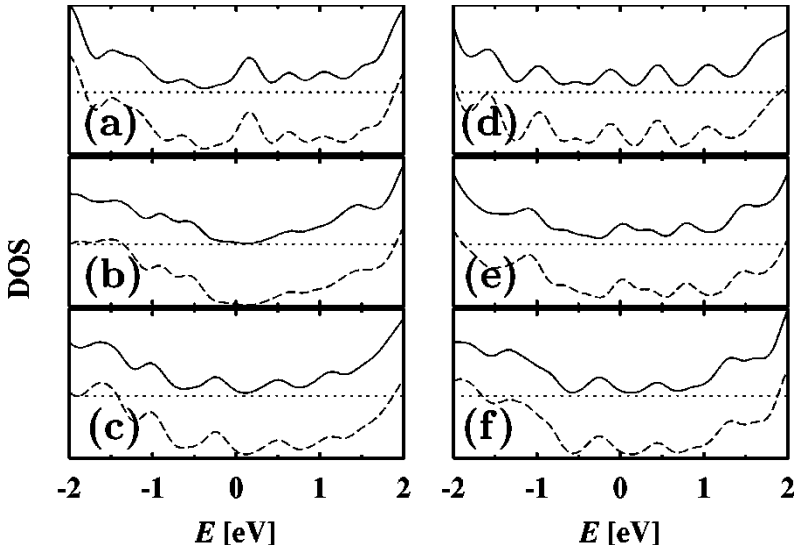

Carbon nanohorn structures with a total disclination angle of 5(π/3), containing five isolated pentagons at the terminating cap. Structures (a)–(c) contain all pentagons at the conical ‘‘shoulder,’’ whereas structures (d)–(f) contain a pentagon at the apex.

Graphite plane

J.C. Slonczewski and P.R. Weiss, Phys.Rev. 109, 272 (1958)

Real space

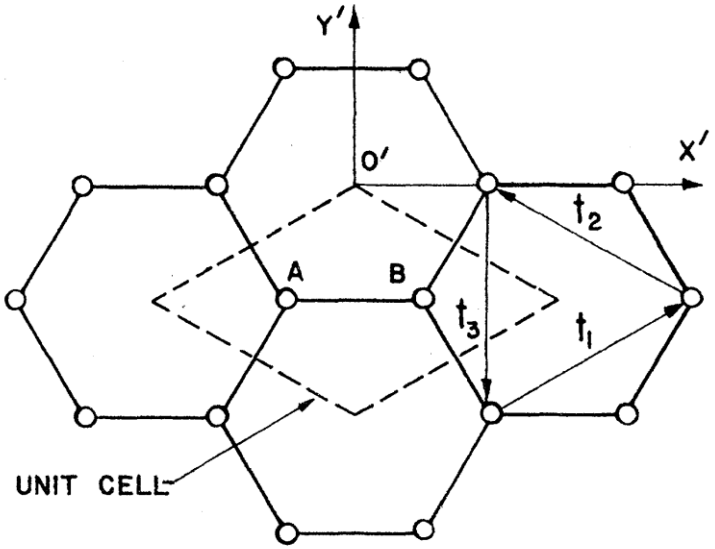

Reciprocal space

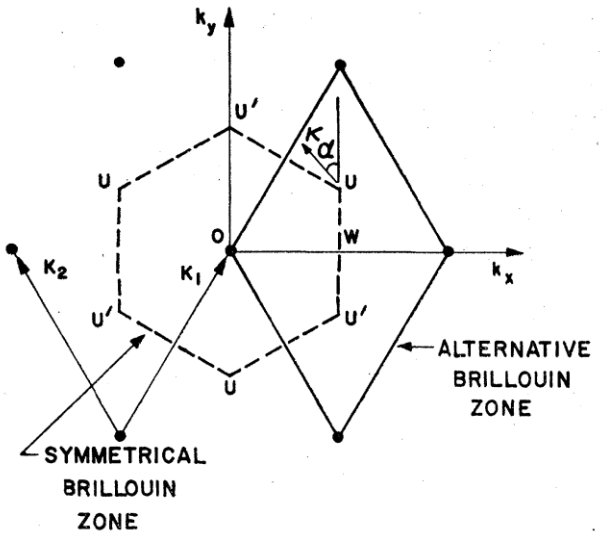

Important:

- there are two atoms per unit cell;
- there are to generate Bloch eigenstates at the Fermi point.

Lattice, spectrum

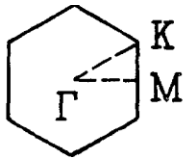

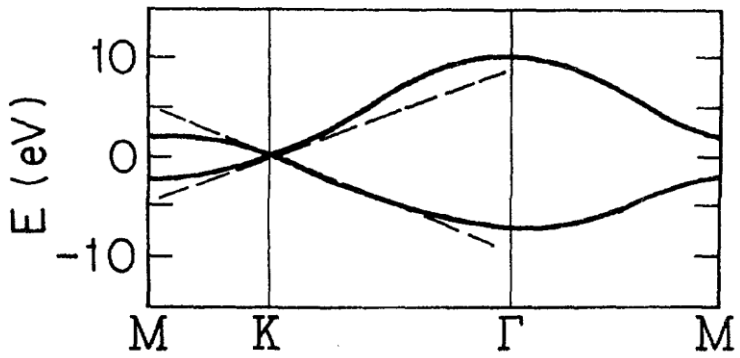

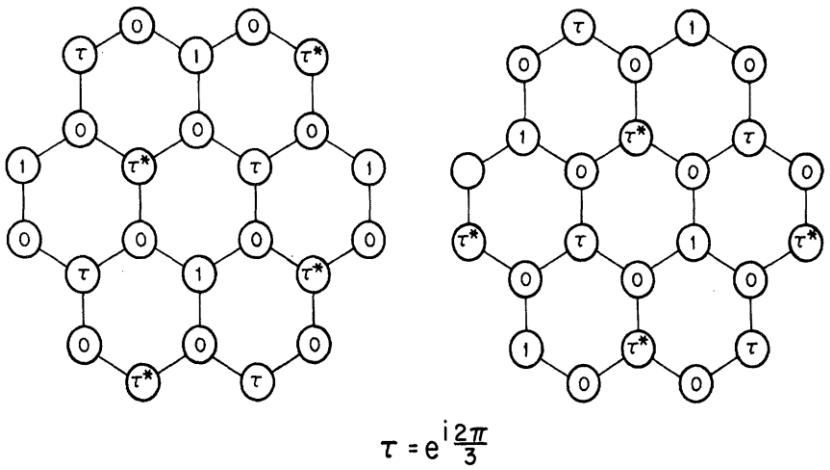

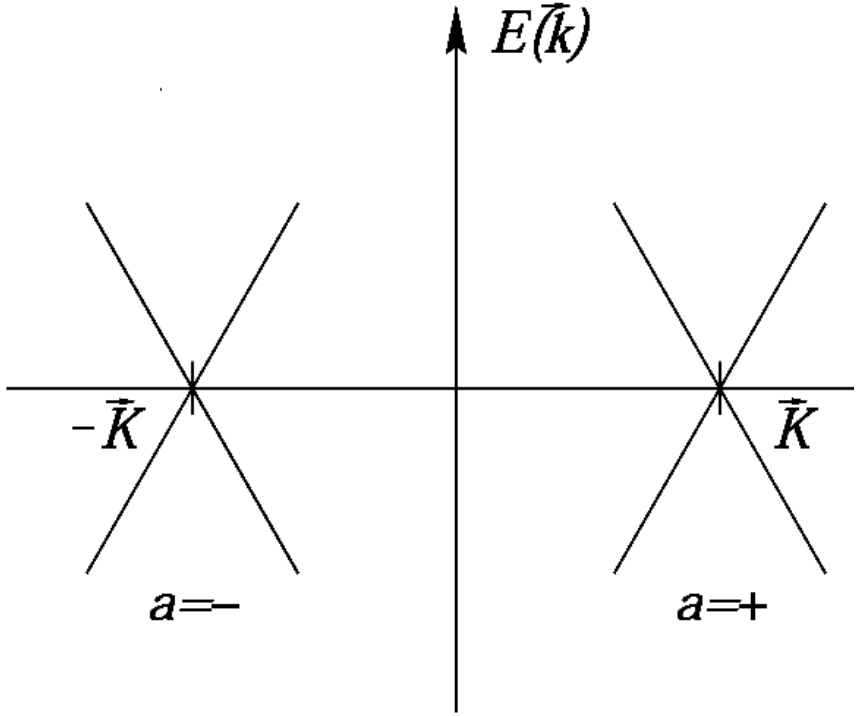

Energy-band structure of the bands of a two-dimensional graphite layer.

Two degenerate eigenstates which provide the basis set for the **kp** trial wave function.

Dirac equation

Step1: the effective-mass approximation, which is equivalent to the kp expansion about the K point in the Brillouin zone

$$\Psi(\boldsymbol{k},\boldsymbol{r}) = f_1(\boldsymbol{k}')e^{i\boldsymbol{k}'\boldsymbol{r}}\Psi_1^S(\boldsymbol{K},\boldsymbol{r}) + f_2(\boldsymbol{k}')e^{i\boldsymbol{k}'\boldsymbol{r}}\Psi_2^S(\boldsymbol{K},\boldsymbol{r})$$

Step2: put it in the Schroedinger equation and diagonalize the secular equation for functions f_i. As a result,

$$\psi = \begin{pmatrix} f_1 \\ f_2 \end{pmatrix}$$

$$-i\sigma^\mu \partial_\mu \psi(\boldsymbol{r}) = E\psi(\boldsymbol{r})$$

The most important fact is that the electronic spectrum of a single graphite plane linearized around the corners of the hexagonal Brillouin zone coincides with that of the Dirac equation in (2+1) dimensions

DOS in 2D

$$DoS(E) = \frac{gV}{4\pi^2} \oint_{\epsilon=E} \frac{dS}{|grad_k \epsilon(\vec{k})|}.$$

g = 4 –degeneracy of electronic states

For linear (Dirac-type) spectrum

$$DoS(E) = \frac{gV|E|}{2\pi},$$

Linear in energy E

Local DOS for arbitrary surface

$$LDoS(E, x) = \Sigma_k |\psi_k(x)|^2 \delta(\epsilon(k) - E)$$

Pedagogical example

Defects in flexible membranes with crystalline order

H. S. Seung and David R. Nelson
Lyman Laboratory of Physics, Harvard University, Cambridge, Massachusetts 02138
(Received 3 March 1988)

We study isolated dislocations and disclinations in flexible membranes with internal crystalline order, using continuum elasticity theory and zero-temperature numerical simulation. These defects are relevant, for instance, to lipid bilayers in vesicles or in the L_β phase of lyotropic smectic liquid crystals. We first simulate defects in flat membranes, obtaining numerical results in good agreement with plane elasticity theory. Disclinations and dislocations eventually exhibit a buckling transition with increasing membrane radius. We generalize the continuum theory to include such buckled defects, and solve the disclination equations in the inextensional limit. The critical radius at which buckling starts to screen out internal elastic stresses is determined numerically. Computer simulation of buckled defects confirms predictions of the disclination energies and gives evidence for a finite dislocation energy.

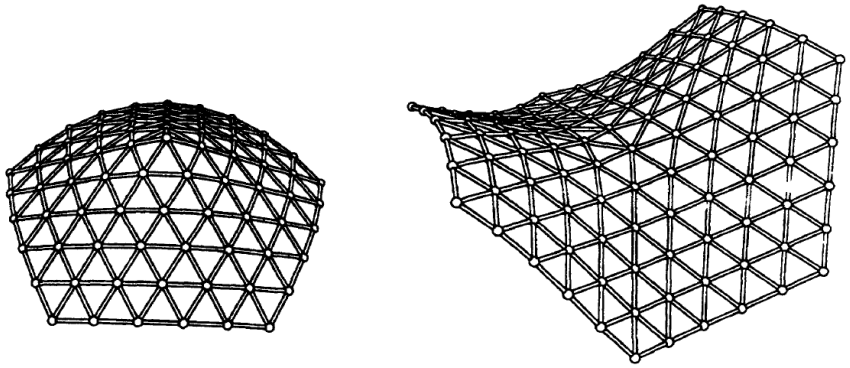

(a) (b)

FIG. 5. (a) Buckled positive disclination ($K_0/\tilde{\kappa}=2000$). (b) Buckled negative disclination ($K_0/\tilde{\kappa}=2000$).

$$\kappa \nabla^4 f = \frac{\partial^2 \chi}{\partial y^2}\frac{\partial^2 f}{\partial x^2} + \frac{\partial^2 \chi}{\partial x^2}\frac{\partial^2 f}{\partial y^2} - 2\frac{\partial^2 \chi}{\partial x\,\partial y}\frac{\partial^2 f}{\partial x\,\partial y}\ , \tag{4.10a}$$

$$\frac{1}{K_0}\nabla^4 \chi + \frac{\partial^2 f}{\partial x^2}\frac{\partial^2 f}{\partial y^2} - \left[\frac{\partial^2 f}{\partial x\,\partial y}\right]^2 = \sum_\alpha s_\alpha \delta(\mathbf{r}-\mathbf{r}_\alpha) + \sum_\beta b_i^\beta \epsilon_{ik}\partial_k \delta(\mathbf{r}-\mathbf{r}_\beta)\ . \tag{4.10b}$$

For a defect-free membrane, the δ-function terms vanish, and we are left with the von Kármán equations for large deflections of thin plates.[19] These coupled nonlinear partial differential equations are "very complicated, and cannot be solved exactly, even in very simple cases."[7]

For an isolated positive disclination at the origin, we assume rotational symmetry and write Eqs. (4.10) away from the disclination core as

$$\kappa \nabla^4 f = \frac{1}{r}\frac{d}{dr}\left[\frac{d\chi}{dr}\frac{df}{dr}\right], \tag{4.11a}$$

$$\frac{1}{K_0}\nabla^4 \chi + \frac{1}{2r}\frac{d}{dr}\left[\frac{df}{dr}\right]^2 = 0, \tag{4.11b}$$

where

$$\nabla^2 = \frac{1}{r}\frac{d}{dr} r \frac{d}{dr} .$$

It is not difficult to guess a trial solution of these equations,

$$\chi = -\kappa \ln\left[\frac{r}{a}\right], \tag{4.12a}$$

$$f = \pm\left[\frac{s}{\pi}\right]^{1/2} r . \tag{4.12b}$$

Although it would appear that we have found an exact solution, comparison with the original form of the von Kármán equations (4.8) reveals that (4.12) is not a true solution because the left-hand side of Eq. (4.8b) is proportional to $\nabla^2\delta(\mathbf{r})$, while the right-hand side vanishes. If we attempt to bypass this issue by deleting a small disk of material around the origin, we create an inner boundary on which σ_{rr} and $\sigma_{r\phi}$ must vanish. One can easily calculate from the expression (4.12a) for χ that σ_{rr} behaves like $1/r^2$, so the inner boundary condition is badly violated if we excise a small disk.

IOP PUBLISHING JOURNAL OF PHYSICS: CONDENSED MATTER

J. Phys.: Condens. Matter **22** (2010) 395502 (11pp) doi:10.1088/0953-8984/22/39/395502

Electronic properties of disclinated flexible membrane beyond the inextensional limit: application to graphene

E A Kochetov[1], V A Osipov[1] and R Pincak[1,2]

Actually, a general solution must include a homogeneous term

$$\chi_0 = -\log\frac{r}{r_0} + q\frac{r}{r_0}$$

The stress tensor takes the form

$$\sigma_{rr} = -\frac{1}{r^2} + \frac{q}{rr_0}$$

$\sigma_{rr}(r = r_0) = \sigma_0$ yields $q = 1 + \sigma_0 r_0^2$

The stretching energy of the membrane

$$E_s \propto \frac{\kappa^2 q^2}{K_0 r_0^2}\log\frac{R}{r_0}$$

Back to the Dirac equation

The Dirac equation on a surface in the presence of the gauge field a_b and the external magnetic field with the vector potential A_b is written as

$$\mathrm{i}\gamma^{\alpha} e_{\alpha}^{b}[\nabla_b - \mathrm{i}a_b - \mathrm{i}A_b]\psi = E\psi$$

with $\nabla_b = \partial_b + \Omega_b$

Schematic densities of states for a small patch near the apex of a cone at zero magnetic field and $K_0 \rightarrow$ infinity

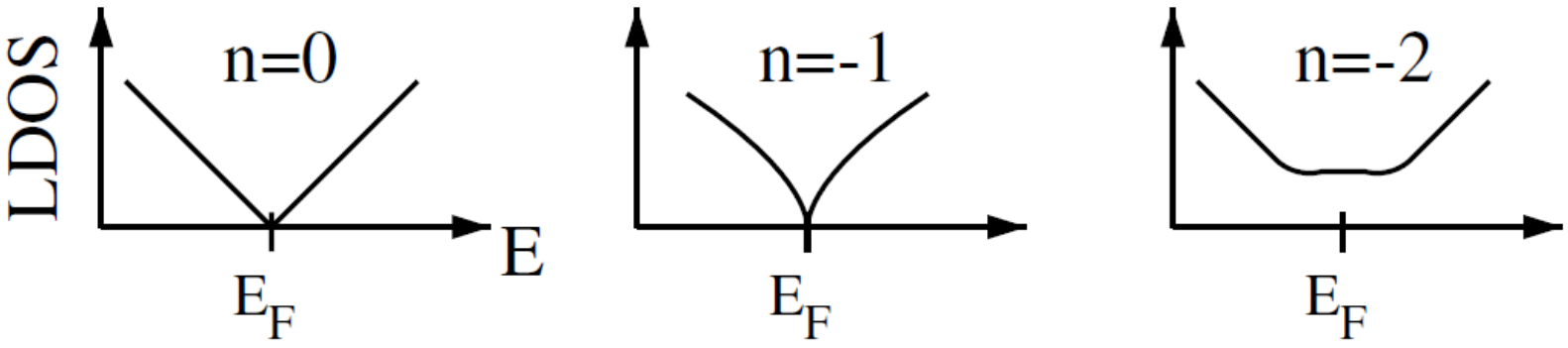

However, a cone with a point-like apex is a mathematical abstraction since in a real situation the media has a finite stiffness, which would inevitably result in a certain smearing of a conical singularity.

Nanocones: another geometry

Upper half of a two-sheet hyperboloid

$$(\chi, \varphi) \to (a \sinh \chi \cos \varphi, a \sinh \chi \sin \varphi, c \cosh \chi)$$

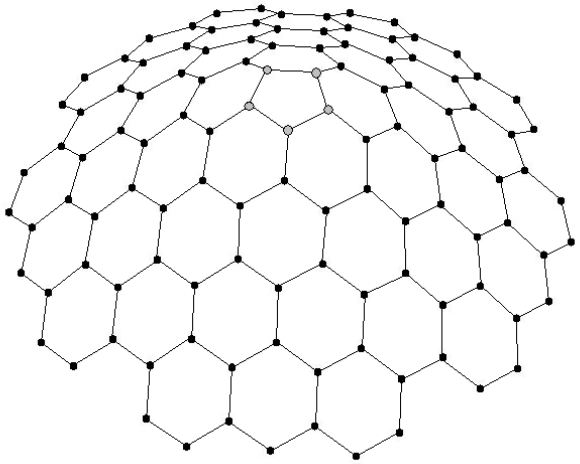

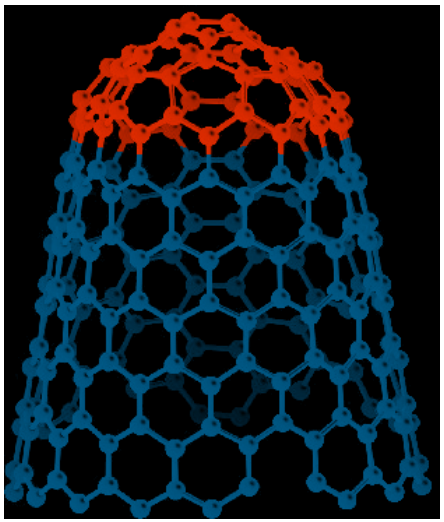

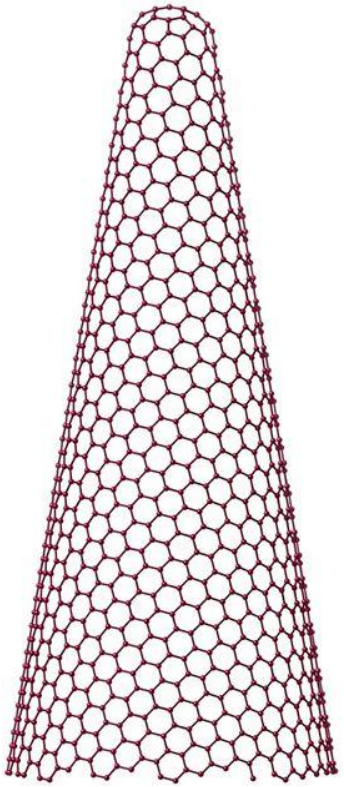

is suitable for the description of cone-like structures with pentagons situated at a smoothed apex. The most appropriate model for nanohorns with five pentagons at the tip.

However, one cannot incorporate finite elasticity into the theory by simply replacing a cone by a smooth surface that asymptotically approaches a cone far away from the origin. This would simply eliminate the defect. To illustrate this, consider an upper half of a hyperboloid as an embedding

$$(\xi, \varphi) \to (a \sinh\xi \cos\varphi, a \sinh\xi \sin\varphi, c \cosh\xi)$$

$$0 \leqslant \xi < \infty, \quad 0 \leqslant \varphi < 2\pi.$$

The components of the induced metric can be written as

$$g_{\xi\xi} = a^2 \cosh^2\xi + c^2 \sinh^2\xi, \qquad g_{\varphi\varphi} = a^2 \sinh^2\xi$$

$$g_{\varphi\xi} = g_{\xi\varphi} = 0,$$

which gives for the spin connection coefficients

$$\omega_{\xi}^{12} = \omega_{\xi}^{21} = 0,$$

$$\omega_{\varphi}^{12} = -\omega_{\varphi}^{21} = \left[1 - \frac{a\,\cosh\xi}{\sqrt{g_{\xi\xi}}}\right] =: \omega(\xi)$$

Since $\omega(\xi)$ goes to zero as $\xi \to 0$ a circulation of that field over a loop encircling the origin gives a flux which tends to zero as the counter shrinks to zero:

$$\lim_{\epsilon \to 0} \oint_{C_\epsilon} \omega_{\varphi}^{12}\, \mathrm{d}\varphi = 0,$$

To incorporate flux we suggest the following metrics

$$g_{\xi\xi} = a^2 \cosh^2 \xi + c^2 \sinh^2 \xi,$$

$$g_{\varphi\varphi} = a^2 \alpha^2 \sinh^2 \xi, \qquad g_{\varphi\xi} = g_{\xi\varphi} = 0,$$

with $\alpha = 1 - \nu$

This metric generates the spin connection term

$$\omega_{\varphi}^{12} = -\omega_{\varphi}^{21} = \left[1 - \frac{a\alpha \cosh \xi}{\sqrt{g_{\xi\xi}}}\right] = \omega_{\alpha}(\xi)$$

and now

$$\lim_{\epsilon \to 0} \oint_{C_\epsilon} \omega_{\varphi}^{12} \, \mathrm{d}\varphi = 2\pi \nu.$$

$$\partial_\xi \tilde{u} - \frac{(j+1/2-a_\varphi+A_\varphi)}{\alpha}\sqrt{\coth^2\xi+\eta}\,\tilde{u} = \tilde{E}\tilde{v},$$

$$-\partial_\xi \tilde{v} - \frac{(j+1/2-a_\varphi+A_\varphi)}{\alpha}\sqrt{\coth^2\xi+\eta}\,\tilde{v} = \tilde{E}\tilde{u},$$

$$\eta \sim \sqrt{\nu\epsilon} \qquad\qquad \epsilon = \kappa/(K_0 r_0^2)$$

The zero-energy mode

$$\tilde{u}_0(\xi) = C(\Delta + k\cosh\xi)^{k\tilde{j}+\frac{\eta\tilde{\Phi}}{2k}}\left(\frac{\Delta+\cosh\xi}{\sinh\xi}\right)^{-\tilde{j}}$$

$$\times\ \exp\left(-\frac{\tilde{\Phi}\Delta\cosh\xi}{2}\right),$$

$$\tilde{v}_0(\xi) = C'(\Delta + k\cosh\xi)^{-k\tilde{j}-\frac{\eta\Phi}{2k}}\left(\frac{\Delta+\cosh\xi}{\sinh\xi}\right)^{\tilde{j}}$$

$$\times\ \exp\left(\frac{\tilde{\Phi}\Delta\cosh\xi}{2}\right),$$

where

$$k = \sqrt{1+\eta}; \qquad \Delta = \Delta(\xi) = \sqrt{1+k^2\sinh^2\xi},$$

$$\tilde{j} = (j + 1/2 - a_\varphi)/\alpha, \qquad \tilde{\Phi} = \Phi/\alpha,$$

Landau states

$$E_n^0 = \pm\sqrt{2n},\, n = 0, 1, 2 \ldots,$$

where the energy is measured in units of $\hbar v_F/l_B$ with the magnetic length $l_B = (\hbar c/eB)^{1/2}$.

$$E_{n=1}^{\eta} \simeq \pm\sqrt{2} \pm \eta\frac{\Gamma}{2\sqrt{2}} \simeq \pm\sqrt{2} \pm 0.3\eta,$$

Landau levels

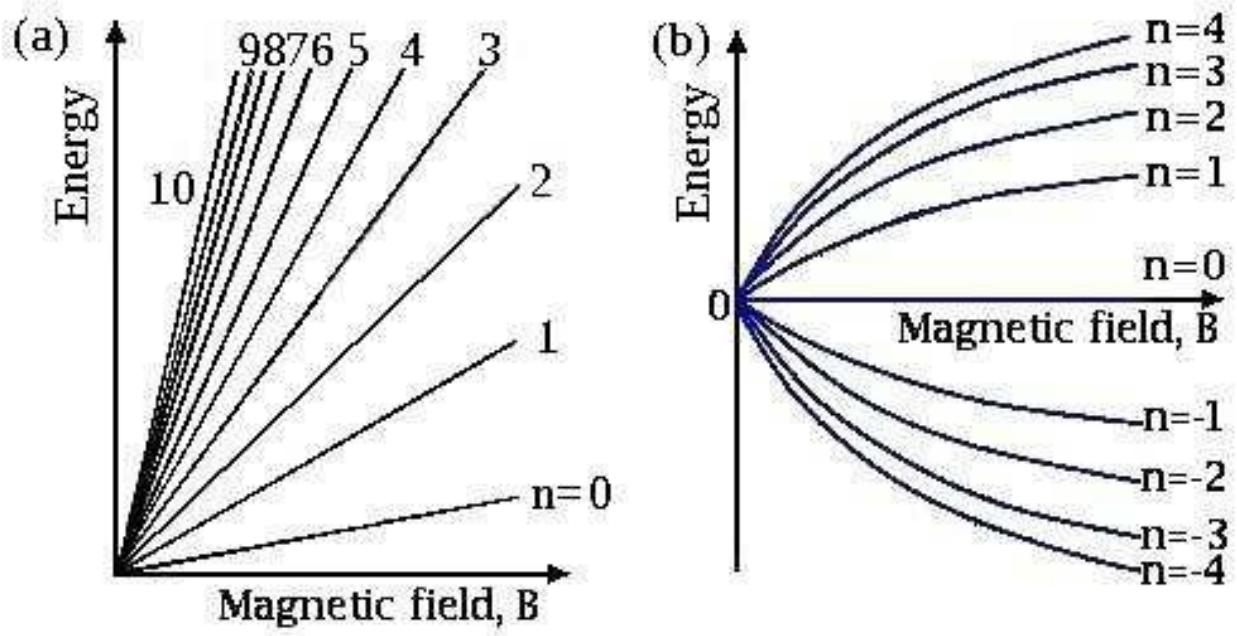

(a) обычные

(b) в графене

Today and tomorrow

- Gap engineering
- Strain engineering
- Metal-Free Molecular Electronics
- GNR-Based Devices with No Analog in Conventional Silicon Electronics

Ribbons

Armchair

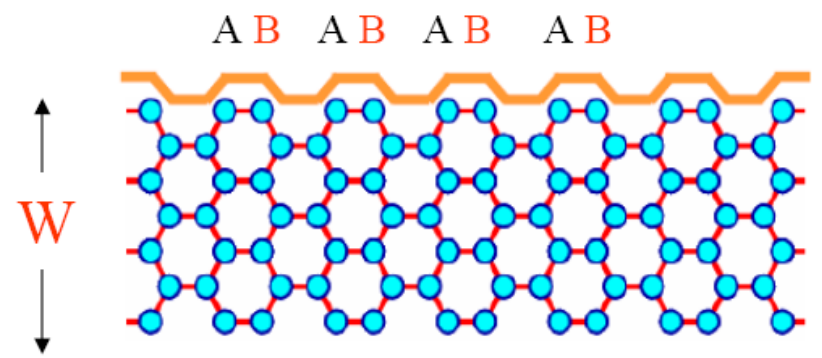

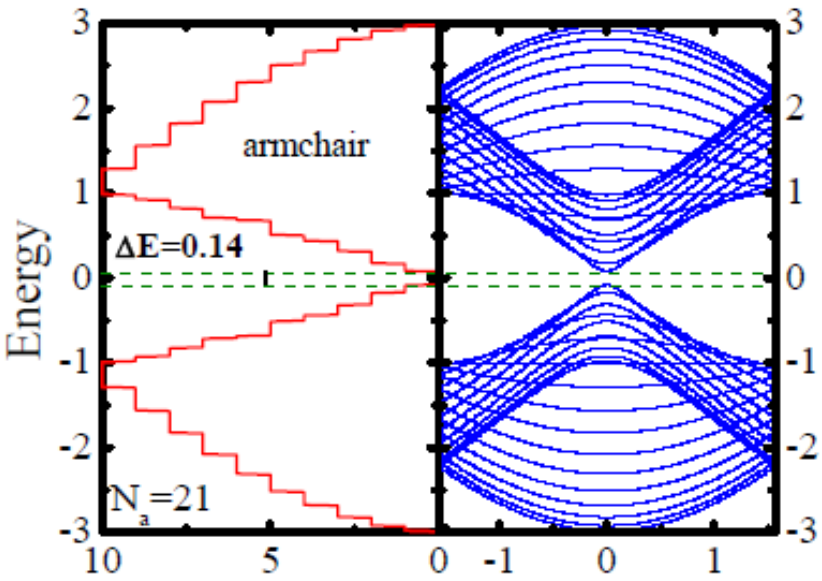

Zigzag